Research Square

Preprints are preliminary reports that have not undergone peer review.
They should not be considered conclusive, used to inform clinical practice,
or referenced by the media as validated information.

Petrogenesis and crustal evolution of Hunza Plutonic Unit, Karakoram batholith, NW Pakistan

Rafique Ahmad

rafique.ahmad@bkuc.edu.pk

Bacha Khan University

Asghar Ali

University of Peshawar

Martin Ondrejka

Comenius University Bratislava

Ondrej Nemec

Comenius University Bratislava

Marián Putiš

Comenius University Bratislava

Matti Ullah

University of Vienna

Nasser Maurad Mahdy

Nuclear Materials Authority

Research Article

Keywords: Karakoram Batholith, I-type granite, Whole rock geochemistry, Mineral chemistry, U–Pb monazite geochronology, Petrogenesis

Posted Date: August 20th, 2026

DOI: https://doi.org/10.21203/rs.3.rs-9269469/v1

License: This work is licensed under a Creative Commons Attribution 4.0 International License.
Read Full License

Additional Declarations: No competing interests reported.

Petrogenesis and crustal evolution of Hunza Plutonic Unit, Karakoram batholith, NW Pakistan

Rafique Ahmad[1,2] . Asghar Ali[1] . Martin Ondrejka[3] . Ondrej Nemec[3] . Marián Putiš[3] . Mati Ullah[4] . Nasser M. Mahdy[5]

1 Department of Geology, University of Peshawar, Peshawar-25130, Pakistan

2 Department of Geology, Bacha Khan University Charsadda, Charsadda-24420, Pakistan

3 Department of Mineralogy, Petrology and Economic Geology, Faculty of Natural Sciences, Comenius University, Bratislava, Ilkovičova 6, 842 15 Bratislava, Slovakia

4 Department of Lithospheric Research, University of Vienna, Vienna, Austria

5 Nuclear Materials Authority, P.O. 530, El-Maadi, Cairo, Egypt

Abstract

The Hunza Plutonic Unit (HPU) and Baltoro Plutonic Unit (BPU) are two the major exposures of plutonic granitoids in the Hunza Valley and Baltoro region in the northern Pakistan. These plutonic units are the eastern and western parts of the southern Asian margin of the India–Asia convergent zone. In this study, the granitoid samples from HPU are studied in detail in term of petrography, whole rock geochemical characteristics, mineral chemistry and U–Pb monazite geochronology. The studied samples essentially consist of quartz, alkali feldspar/plagioclase, hornblende, biotite, muscovite, garnet, well developed myrmekitic textures and accessory to trace amounts of sphene and zircon. According to monazite U–Pb dating, the HPU Karakoram Batholith granitoid was emplaced around 34 ± 2.2 Ma ranges from 21 to 64 Ma which represents the post–collisional magmtism in the Karakoram Block. Variations in major and trace element contents indicate evolution of the HPU of Karakoram Batholith through magmatic differentiation. Geochemically the investigated samples span from ferroan to magnesian, calcic to alkaline and peraluminous to metaluminous. According to the normalized primitive mantle results these samples exhibit enrichment in large–ion lithophile elements (LILEs) such Cs, Rb, U, and K, and light rare earth elements (LREEs) in comparison to Nb and also simultaneous depletion in Ti. The parent melt most likely originated from a source enriched in LREEs which show enrichment in LREEs [$(La/Sm)_N$ = 1.62–10.92] as compared to HREEs [$(Tb/Yb)_N$ = 1.2–5.3]. The samples also show low to moderate quantities of Fe^{2+} in their biotite ($Fe^{2+}/(Fe^{2+} + Mg)$ = 59%–68%. The stability and composition of biotite in the anninite series are influenced by the

total Fe content and its oxygen fugacity. However, lower oxygen fugacity and temperature are the main causes of the enhanced Fe levels in biotite rather than a larger bulk Fe concentration. The significant variation in Fe # values of biotite reflects the fluctuation in oxygen fugacity conditions. After biotite crystallization at temperature 625 °C and 695 °C, plagioclase fractionation is further supported by the negative correlation between SiO_2, CaO, and Sr which is thought to occur at temperatures ranging from 703 °C to 1066 °C . Overall the granitoids of the HPU are classified as I–type granite, which can be clearly seen in a decreasing trend of P_2O_5 as SiO_2 increases.

Keywords Karakoram Batholith . Petrography . Whole Rock Geochemistry . Mineral Chemistry . U–Pb monazite Geochronology . Petrogenesis

Introduction

The Hindu Kush and Karakoram plates were the dominant parts of the southernmost margin of the Asia before India–Asia collision. These two terranes are geologically equivalent to the Lhasa block in the south Tibet (e.g., Searle and Khan 1996). The south Tibet within the Tibetan Plateau exposed mainly the volcanic and sedimentary rocks of the upper crust to the surface. The Karakoram Range comprises of thick crustal high mountains with 8 km rising peaks and deeply incised valleys which experience high erosion rates (Searle 1991). This linear belt of high mountains in the Karakoram Range resulting from rapid uplifting of thick continental crust (65 – 70 km; Zeitler, 1985; Searle et al. 1988; Molnar and Lyon-Caen 1989).

The exposed Karakoram orogenic belt of the Gondwana affinity in Pakistan provides a natural laboratory to understand syn– and post– tectonic magmatism, multiple phases of metamorphism and deformations associated with sequential collision of plates and closing of the intervening oceans (Gaetani 1997; Hildebrand et al. 1998, 2000, 2001). The Rushan–Psart suture zone separates the Karakoram from the Hindu Kush whereas the Shyok Suture Zone also called Main Karakoram Thrust delineates the southern plate boundary with the Kohistan Island Arc (KIA) (Searle 2011; Hacker et al. 2005; Kooijman et al. 2017).

The formation of Himalaya resulted from the collision of KIA with Indian plate and then Asia along the Indus suture zone which occurred the crustal thickening and uplifting along the southernmost margin of the Asia (Hindu Kush–Karakoram–Lhasa and Qiangtang terranes of Tibet; Searle et al. 1999). The important phases of pre–collisional metamorphic, magmatic and deformational activities as well as Tertiary post–collision orogenic effects are studied in the

Hindu Kush (Hildebrand et al. 1998, 2000, 2001), Karakoram (Searle et al. 1989; Searle 1991; Fraser et al. 2001) and Pamir (Robinson et al. 2004, 2007; Schwab et al. 2004) ranges. These Karakoram–Hindu Kush–Lhasa and Qiangtang orogenic terranes (Searle et al. 1999; Palin et al. 2012; Larson et al. 2019; Soret et al. 2019) resulted in the regional kyanite and sillimanite grade metamorphism culminating in the Early Miocene partial melting and generation of crustal melt leucogranites along the Indian Plate in Himalaya (e.g. Searle et al. 1999, 2003, 2006; Hodges 2000; Law et al. 2006) and southern margin of the Asian Plate in the Karakoram (Searle 1991; Searle and Tirrul 1991; Fraser et al. 2001). The effects of magmatic activities during the India–Asia collision following the Early Eocene are well known along the Indian Plate in the Himalaya but are less well known along the Asian margin.

Three major and successive subduction related tectonic events have been documented in the Karakoram terrane. The Karakoram basement rocks are intruded by the Cretaceous calc–alkaline plutonic axial batholith (Crawford and Searle 1992; Debon and Khan 1996; Debon et al. 1987). This event also led to the Mid–Cretaceous opening of the Shyok back–arc basin (Rolland et al. 2000, 2002). The complete closure of the intervening Paleo–Tethys between the KIA and Karakoram microplate in the Late Cretaceous preserved in the form of the Shyok Suture Zone (Petterson and Windley 1992; Rolland et al. 2000; Weinberg et al. 2000). The final closure of the intervening Neo–Tethys between the KIA and the Indian Plate in the Eocene caused crustal thickening, mid crustal anatectic melting and amphibolite facies metamorphism in the Karakoram microplate (Rolland et al. 2001; Mahéo et al. 2004; Zhu et al. 2005; Green et al. 2008; Searle et al. 2010).

The origin of peraluminous granites is usually resulted from melting of the crustal pelitic rocks (Clemens and Wall 1984; Todd and Shaw 1985; Stuckless 1989) through prevailing partial to complete melting reactions, 1) muscovite dehydration melting at ~620–650 °C (Thompson 1982), 2) lacking or deficient fluid muscovite break down melting at ~700–750 °C (Harris et al. 1995) and 3) without fluid melting of biotite at approximately 750 °C (Le Breton and Thompson, 1988). The structure relations and whole rock isotopes analyses for Rb, Nd, Sr, and O (e.g., Deniel et al. 1987) are reliable with crustal origin. The comprehensive research has been completed on partial melting of the subducting Indian plate, while insufficient studies were performed on the Asian plate partial melting succeeding crustal thickening.

Furthermore, depends on Pb, Nd and Sr isotopic composition, monazite and zircon inheritance, Schärer et al. (1990) suggested a robust crustal input; i.e. approximately > 70% of

the magmas are resulting from the metasedimentary rocks of the Karakoram Metamorphic Complex (KMC). Similarly, partial melting of the deep seated granodiorite to dioritic and metabasalts (Cretaceous and calc–alkaline rocks) has been suggested (Mahéo et al. 2009). Thus, several sources have been suggested for these rocks having similar whole rock isotopic nature.
From these past researches, it is clear that the detailed description of magma source components and petrogenetic procedures for the generation of post collisional granites and related rock from batholith is difficult to oblige by whole rock geochemistry and isotopes related data. Such results provide average evidence and are subtle to post – crystallization, chemical and mineralogical modification (e.g., Hawkesworth and Kemp 2006; Kemp et al. 2007; Appleby et al. 2010). The ability to explore the micro scale in-situ U–Pb and Lu–Hf isotopic records of zircons has transformed granite, granodiorite, syeno–granite petrology, particularly with reference to the history of magma mixing and source region (e.g., Goodge and Vervoort 2006; Kemp et al. 2005, 2009a; Shaw and Flood 2009; Zeh et al. 2007). However, the Hf isotopic system alone sometimes is not able to constrain the participation of mantle magmas in granite petrogenesis (e.g., Hawkesworth and Kemp, 2006; Kemp et al. 2007, 2008). The oxygen isotopic record from zircon grains delivers more robust constraints to examine the contribution of mantle–derived magmas (Valley et al. 2005) in plutonic igneous rocks formation (Appleby 2008; Gagnevin et al. 2011; Miles et al. 2014 and references therein).

Due to the lack of strong supporting evidences for either the direct impact or the subduction of the Indian Plate beneath the southern margin of the Asian plate, the explanations appear puzzling. There are substantial doubts regarding post–collisional magmatism due to the unarguable evidence in earlier theories on the origin and emplacement of I-type granitoids of the Hunza Plutonic Unit (HPU) in the Karakoram Block. To fill in the gap from the previous studies, the petrographic characterization, whole rock geochemistry, mineral chemistry and U–Pb monazite dating have been used here to govern the emplacement age of HPU granitoids and the relative constituents of mantle and crustal sources. Our research provides a new petrogenetic framework that explains subduction zone magmatism in the Hunza valley (Fig. 1) as compared to KIA granitoids and Khunjerab granitoids in the south and north respectively. Our model also explores the evolution of the Himalaya–Karakoram orogenic system and the subduction dynamics of the Tethys.

Geological Background

The Hunza Valley in the north Pakistan (Fig. 1) provides an outstanding and accessible profile across the KMC and plutonic rocks to its north. Mapping along the valley by Crawford (1988), Rex et al. (1988), Searle (1991), Crawford and Searle (1993) showed the southward thrusting of the Karakoram batholiths units over the sillimanite gneisses of the KMC.

Lithologically, the Karakoram batholith of the HPU in the Hunza Valley is mostly composed of quartz diorite and granodiorite. These deformed collision-related rock units have been dated as 95 +4/6 Ma (U–Pb, Le Fort et al. 1983) and 97±17 Ma (Rb–Sr, Debon et al. 1987). Granodiorites were later intruded by multiple sets of dikes termed as Hunza dikes which represent a complex cogenetic suite of granodiorite, monzogranite to garnet + muscovite ± biotite leucogranite (Crawford 1988; Crawford and Searle 1993). Many of these dikes have been strongly deformed and rotated into an E-W-striking, N-dipping alignment by simple shear during south-vergent thrusting (set 1 Hunza dikes), but some undeformed dikes (set 2 Hunza dikes) crosscut the fabric, both in the granite batholith and the sillimanite gneisses to the south (Fraser et al. 2001).

Analytical Techniques

To determine the monazite age, one granitic sample (RA–I–32) was chosen with 45 analyzed spots in monazite grains to ensure the precision of the data. Geochronology of monazite was carried out by the monazite age reference correction (MARC) method developed in the Dionýz Štúr State Geological Institute in Bratislava (Konečný et al. 2018). This method is using microprobe analyses from the CAMECA SX 100. Monazite spot analyses were acquired under 15 kV accelerating voltage, 180 nA beam current, and a 3 μm beam diameter with the aim of increasing both counting efficiency and spatial resolution. Long counting times were used to increase the analytical precision: for Pb (300 s peak and 2×150 s backgrounds), Th (35 s peak and 2×17.5 s background), U (80 s peak and 80 s background), and Y (40 s peak and 2×20 s background). A set of 10 reference standards was utilized for assessment of minor systematic errors that cannot be suppressed in the currently used measuring procedure, but are accumulated regardless of the number of analyses. Other details and principles of MARC dating technique can be found in Konečný et al. (2018).

The whole rock geochemical analyses for selected samples were performed at James Cook University; Townsville, Australia using Scanning Electron Microscopy-Energy Dispersive X-ray Spectroscopy (SEM–EDS) for major elements, Laser ablation–inductively coupled plasma –

mass spectrometry (LA–ICP–MS) for the trace and REEs. Using the EPMA techniques, elemental mapping and analyses of different mineral phases were acquired CAMECASX100 equipment at the Department of Electron Microanalysis at the State Geological Institute of Dionýz Štúr, Bratislava, Slovak Republic. The electron probe micro analyser has four spectrometers and large surface LLIF and LPET analysing crystals which provide approximately four times more sensitivity than conventional EPMAs. An accelerating voltage of 15 kV was used for all mineral phases. Analytical conditions were adapted according to mineral type. The most common spot beam diameter varied from 5 to 10 μm, a more focused and less refractory 3–5 μm beam was also utilized. Higher current gave the optimal count rate for trace elements and excitation of less intense analytical lines such as REE. Feldspar as analyzed with 10 nA. Allanite and LREE were analyzed with 30 nA while apatite and zircon were analyzed at 20 nA.

Results

Petrography

Quartz occurs as euhedral to subhedral and commonly medium to large size grains; however, small grained quartz also occurs in some of the samples (Figs. 2a, b). Some of the quartz grains display undulose extinction. Myrmekitic intergrowths of quartz in plagioclase and in some cases orthoclase along with plagioclase are very common. In some cases quartz is mildly fractured and resorbed at margin having inclusions of opaque minerals (Fig. 2c).

All the studied samples contain biotite and muscovite. Bioitite is the common mafic minerals of the studied samples. Some of the biotite grains display brown color most probably due to leaching and oxidation of iron (Fig. 2a). Most of the Biotite grains lie in parallel position with the muscovite flakes. Fine-grained muscovite (sericite) is a common alteration product of plagioclase. The plagioclase also hosts the muscovite inclusions. The muscovite laths are well oriented within a titanite. In some cases plagioclase is partially replaced by muscovite.

Plagioclase grains are euhedral to subhedral, exhibit albite and carlsbad polysynthetic twinning. Some of these grains undergo such drastic changes that they lose their original optical characteristics (Figs. 2b, c). In addition, the plagioclase grains also show intracrystalline deformation, such as bending, twin lamellae microfolding and kinking, and patchy and undulose extinction (Fig. 2c).

Potash feldspar occurs as subhedral to euhedral coarse grain crystals surrounded by biotite, muscovite and quartz (Figs. 2a, b). Some of the potash feldspar grains seem blurred, and due to brittle deformation they look pulled apart and the fractures are filled with micro

crystalline quartz (Fig. 2a). Amphibole (hornblende) is dominant component in some of the samples with crushed grains into tiny crystals. These grains mostly represent reaction texture. The amphibole grains are subhedral to anhedral and dispersed in cluster form mostly associated with biotite flakes (Fig. 2d).

Minor to accessory quantities of epidote, zircon, titanite, allanite and apatite are present in the studied samples (Figs. 2e, f). Epidot and allanite intergrown with each other where the allanite is wrapped around by former one in some samples (Fig. 2e). Further, the epodite grains are mostly sheared, cracked and broken at margins. Zircon mostly occurs as inclusion in muscovite and very rare in biotite. Apatite is mostly present in the form of well-developed elongated crystals with randomly oriented in some of the studied samples (Fig. 2f). Monazites occur as angular-to-rounded crystals mostly associated with allanite and apatite. These monazite grains are studied in two samples.

Whole-rock geochemistry

The whole rock geochemical results are given in table 1. The studied samples contain variable amounts (wt. %) of SiO_2 (54.56–71.20), TiO_2 (0.14 – 1.65), Al_2O_3 (14.30 – 19.40), FeO_{tot} (1.10 – 7.84), MnO (0.02 – 0.15), MgO (0.39–5.33), CaO (1.13–9.02), Na_2O (2.75 – 4.09), K_2O (1.26 – 5.88) and P_2O_5 (54.56–71.20; Table 1). The major oxides and SiO_2 are also utilized for the classification and determination of geochemical behavior of selected samples (Fig. 3a–d). Based on the classification in the total alkali vs silica (TAS) diagram (Cox et al. 1979), the samples plot in granite, diorite, granodiorite and syenite (Fig. 3a), reliable with petrographic observations. According to the geochemical characterization, all the studied samples varies from slightly ferroan (granite, granodiorite and syenite) to magnesian (granite and diorite; Fig. 3b), and from alkalic to calcic (Fig. 3c). The rocks are metaluminous to peraluminous with their A/CNK and A/NK ratios ranging from 1.3 to 1.8 and from 1.5 to 3.7 respectively (Fig. 3d).

The total rare earth element (∑REE) contents of studied samples show a gradually increasing trend (177–67 ppm; Fig. 4). In general, the samples have patterns that slope right from LREE (La–Pm) to MREE (Sm–Gd), but HREE (Tb–Yb) has a flat pattern show high light to heavy REE fractionation ratios [$(La/Yb)_N$ = 2.8–152.63; Table 1; Fig. 4a). The values of Eu anomalies (Eu_N/Eu^*)] range from moderately negative to positive (0.64–1.2; Table 1). Overall studied samples exhibit enrichment of immobile HFSE (e.g. Nb) and depletion of Pb and LFSE especially Rb, Ba, Cs, and Sr (Fig. 4b). According to Whalen et al. (1987), the representative granitoid samples fall in fractionated granite and unfractionated granite fields (OTG; Fig. 5a, b).

Similarly According to Pearce et al. (1984) Rb vs. Y+Nb discrimination diagram, the selected samples are clearly classified as volcanic arc granitoids (VAG; Fig. 5c). But the negative correlation of SiO_2 with P_2O_5 in almost in all samples more likely suggests an I- type granite affinity (Fig. 5d; Chappell 1999).

The samples show enrichment in large–ion lithophile elements (LILEs) such Cs, Rb, U, and K, as well as light rare earth elements (LREEs), in comparison to Nb, when normalized to the primitive mantle (Fig. 4). They display depletion in Nb, and Ti at the same time, which is similar to Cretaceous granitoids found in Kohistan batholith and Khunjerab pluton (Ullah et al. 2025). The parent melt most likely came from a source enriched in LREEs, according to the REE data for the HPU, which show enrichment in LREEs [$(La/Sm)_N$ = 1.62–10.92] as compared to heavy REEs [$(Tb/Yb)_N$ = 1.2–5.3] (Table 1).

Mineral Chemistry

The analyzed biotites from three samples show molar Fe/(Fe + Mg) ratio of 0.59 to 0.68 (Table 2). According to Deer et al. (1992) and Tischendorf et al. (1997), all the biotite composition corresponds to annite-siderophyllite (Fig. 6a, b). Using the MgO–FeOt–Al_2O_3 (Abdel-Rahman 1994) classification, the biotites composition fall in the peraluminous suite field with little inclination towards calc-alkaline orogenic suite (Fig. 6c). Ti is present in trace amount (0.29 to 0.46 apfu). The biotites from the studied samples seem Fe- and Ti- rich and Cl- poor with no F.

The chemical composition of analyzed plagioclase and potash feldspar represents sodium end member of plagioclase (albite) and potassium end member of the alkali feldspar series (orthoclase). The representative feldspars from one granodiorite sample correspond to albite ($Ab_{67–63}An_{32–36}$) while the two granite samples correspond to orthoclase ($Ab_{2–81}Or_{0.5–97}$ and $Ab_{5.4–84.8}Or_{0.2–94.5}$; Fig. 6d, Table 3).

Monazite-(Ce) chemistry and geochronology

Monazite-(Ce) is a relatively abundant accessory mineral in the studied sample RA–I–32. It is equally distributed throughout the granite and is primarily found in association with biotite. They are anhedral to subhedral ≤20 μm in size with occasionally uneven highly embayed grain boundaries. In some grains, the dark domains in the middle region are overgrown and consumed by later brighter monazite. In some cases the irregular reaction rim replace the monazite to varying degree ranging from partial replacement to moderate replacement depending on the location of both host mineral (monazite) and replacing minerals (allanite and xenotime-(Y)) (Fig. 7).

The analyzed monazite grains represent the dominant LREE phosphate end-member composition and contain only minor amounts of the cheralite ($–Ca_2Th_2(PO_4)_4$) and huttonite ($-ThSiO_4$) components (Table 4). It shows predominance of LREEs, where Ce^{3+} is the dominant REE cation (0.35–0.40 apfu Ce). Thorium content ranges from 7.0 to 11.9 wt.% ThO_2 (0.09–0.01 apfu Th). Similarly, Ca concentration varies from 1.1 to 2.2 wt.% CaO (0.02–0.1 apfu Ca) and Si ranges from 0.3 to 1.3 wt.% SiO_2 (0.01–0.05 apfu Si). The change in mineral chemistry is mostly controlled by both huttonite $(Th,U)Si(REE,Y)_{-1}(P)_{-1}$ and cheralite $Ca(Th,U)(REE,Y)_{-2}$ substitutions. (Figs. 8a, b). The increase in Th concentration is compensated by elevated U and Y i.e. 0.1.6–1.24 % UO_2, 0.30–2.07 Y_2O_3 %. The concentrations of the elements As, S, Sr, and Fe which usually participate in monazite composition are very low or below the detection limit (Table 4; Fig. 8a). A total of 7 monazite grains from sample RA–I–32 (granite) are targeted for in situ U–Th/Pb analyses (Table 5). The relatively high content of actinide elements enables EPMA in situ U-Th-Pb dating of monazite-(Ce), which represent their primary crystallization ages. The application of this method on monazite from the HPU delivered the age of 34±2.2 Ma (Fig. 8b).

Discussion

Genetic type of the HPU Granitoids

The discrimination of I- and S-type granites is related with derivation from igneous and sedimentary protolith (Chappell and White 2001). These two kinds may be effectively distinguished by using mineralogical indicators, such as the high modal abundance of ferromagnesium silicate phases (mostly amphibole, pyroxenes, and biotites) in I-type granites and Al-rich phases (garnet, muscovite, tourmaline, and cordierite) in S-type granites. Furthermore, according to Chappell and White (2001), I-type granites are typically metaluminous with A/CNK values less than or closer to 1.0, while S-type granites are highly peraluminous with A/CNK values more than 1.1. The HPU granitoids samples are reported as Fe/Mg-rich phases (biotite and hornblende; Fig. 2) and are metaluminous to slightly peraluminous. They have high CaO and MgO + FeO_{tot} contents, indicating the affinity to I-type granites (Fig. 5a, b). Moreover, in some cases, intense differentiation of I-type granitic magma can result in strongly peraluminous for the residual melt (e.g. Liu et al. 2014; Wu et al. 2016). Similarly in some of the HPU granitoid samples, biotites are associated with allanite and titanite (Fig. 2d) indicating the oxidized character of I-type granite (Petrík and Broska 1994; Petrík and

Kohút 1997). The HPU granitoids exhibits a limited range of variations in both major and trace element contents. Thus, the HPU granitoids granite belongs to I-type.

Mineralogical Characterization, Geochemical Affinity and comparison with worldwide Granites

The presence of mafic and accessory mineral assemblages e.g. biotite, amphibole, zircon, ilmenite, titanite, and epidote (Fig. 2) in the studied samples show similarity with ferroan to magnesian, alkali to calcic and metaluminous to peraluminous rocks elsewhere in Pakistan (Ullah et al. 2025 and references therein). The petrographic signature and chemical behavior of biotite (cf. Whalen et al. 1987) in the studied samples are comparable to some well documented metaluminous to peraluminous rocks I–type granites from other parts of the world (Figs. 5a, b; 6a, b, c). For instance, the presence of Fe-rich biotite and accessory mineral assemblages in the studied granitoids are similar to the I-type Early Paleozoic granitoids in the Boshan deposits of South China (Lyu et al. 2024), Dongyuan deposits, Anhui Province, China (Zhang et al. 2021), Jirang–Patharkhamah, Meghalaya India (Gogoi and Bhagabaty, 2022) Araçuaí orogen, SE Brazil (dos Santos Dias et al. 2019) and Khunjerab Pluton, north Pakistan (Ullah et al. 2025). Furthermore, mineral assembalges of the HPU granitoids are similar to that of the Boshan deposits, Dongyuan deposits, Araçuaí orogen, SE Brazil and Khunjerab Pluton (dos Santos Dias et al. 2019; Lyu et al. 2024; Ullah et al. 2025).

The water concentration of ~4.0 wt. % at 2.6–3.5 kbar (Fig. 9) is estimated from the biotite chemistry (cf. Ridolfi, 2021 and referencen therein). The samples also show low to moderate quantities of Fe^{2+} in their biotite ($Fe^{2+}/(Fe^{2+} + Mg)$ = 59%–68% (Table 2). Both the fO_2 and the total Fe content of the rock affect the stability and composition of biotite in the annite series. Similarly the fO_2 value varies in magnetite-free and magnetitite-bearing granitoids. However, lower oxygen fugacity and temperature are the main causes of the enhanced Fe levels in biotite rather than a larger bulk Fe concentration (Fig. 9; cf. dos Santos Dias et al. 2019). The Fe # values of biotite (Table 2) vary significantly, reflecting fluctuating oxygen fugacity conditions (Fig. 9). These geochemical features, especially the biotite compositions, suggest that low oxygen fugacity conditions were present during the crystallization of the HPU granitoids. Additionally, the EPMA based chemistry of the feldspar and plagioclase include Na end member of plagioclase (albite) and potassium end member of the alkali feldspar series (orthoclase) (Fig. 6d).

Amphibole (hornblende; Fig. 2d) crystallizes first in a discontinuous reaction series, followed by biotite, which according to the studied samples crystalized above 500 °C and in between 625 °C and 695 °C (Fig. 9; Table 2; Henry et al. 2005). Plagioclase fractionation is further supported by the negative correlation between SiO_2, CaO, and Sr, which is thought to occur at temperatures ranging from 703 °C to 1066 °C based on EPMA data using the method of Kudo and Weill (1970).

Plagioclase crystallization is indicated by the Eu anomalies in some samples from the HPU (Fig. 4a). According to tectonic discrimination diagrams, the pluton was evolved in an active compressive orogenic environment inside a volcanic arc granitic (VAG) region. The granitoid of the HPU is classified as an I–type granite, a crucial signal for differentiating between S–type and I–type granites and can be clearly seen in a decreasing trend of P_2O_5 as SiO_2 increases (Fig. 5d). Further, apatite reaches saturation in metaluminous and mildly peraluminous magmas when the aluminum saturation index (A/CNK) is less than 1.1, although it dissolves more easily in strongly peraluminous melts (Wolf and London 1994). This pattern is consistent with the usual evolutionary traits of I–type granitoids, as reported by Chappell (1999), Cao et al. (2016), Ali et al. (2024), and Ullah et al. (2025). However, Gao et al. (2016) contend that the correlations between A/CNK and SiO_2, P_2O_5 and SiO_2, or Na_2O, K_2O and CaO as well as trace elements like Zr, Ce, Nb, Y, and Ga, cannot be used to categorize granites. This is because the major and trace element compositions of granites are greatly influenced by a number of magmatic processes, including fractional crystallization and partial melting, which were key in the formation of the majority of the HPU granitoids, as a result, lithochemical correlations by themselves could produce unclear findings about the origins of granite. In arc settings, connected to subduction, intermediate to felsic I–type magmatism is often formed by two main causes. Firstly, the parent magma in the crust crystallizes fractionally (Grove et al. 1997, 2003; Wu et al. 2016) while second mechanism involves the mixing of partially melted, hydrous basaltic magma from the heated mantle wedge with lower crustal material to create hybrid magma. The second mechanism supported the origin of I-type HPU granitoids.

Enrichment in LILE relative to high-field-strength elements (HFSE) like Nb, and Ti, as well as in LREE relative to HREE are geochemical characteristics of the Karakoram batholith magma (Fig. 4b). A metasomatized mantle wedge effected by fluid or melt contributions from the subducting plate is suggested by these geochemical markers as well as high La/Nb (2–13.5), Sr/Nd (12–20), and Ba/Nb (42–169) ratios (calculated from Table 1; Chilson-Parks et al. 2022).

Therefore, it is assumed that the metasomatized mantle that underwent change as a result of subduction-related activities is the magma source of the HPU of Karakoram Batholith. The observed geochemical variations are thus explained by the interpretation of the magma source as a mantle wedge over an active subduction zone that underwent differential metasomatism.

Chronological Constraint of HPU

The ages for igneous suits of Karakoram batholith show signification variation. For instance, 111.5 – 41 Ma (U–Pb zircon; Heuberger et al. 2007; Ullah et al. 2025) and 102 – 41 Ma (Rb-Sr, whole rock; Heuberger et al. 2007; Ullah et al. 2025) ages have been assigned in different times to the igneous suits in north Pakistan. Similarly the ages of plutonic and volcanic rocks in the north of Karakoram Batholith (Khunjerab Pluton) are reported as old as 141 Ma (Schaltegger et al. 2002; Ullah et al. 2025) while quartz–diorites, basaltic sills, and granite dikes of Kohistan region have ages of 107 Ma and 112 Ma (Ogasawara et al. 2004, Heuberger et al. 2007). Schärer et al. (1984) and Khan et al. (2009) reported the youngest zircon ages (~ 61 Ma) for granites in Ladakh. Pingal pluton within the Kohistan Batholith yielded U–Pb zircon ages of about 41 Ma (Heuberger et al. 2007; Khan et al. 2009) which suggest that the tectonic and magmatic processes of the Karakoram–Kohistan Suture Zone continued until the Eocene. These findings reveals that tectonic activity continued ca. 50 Ma ago in the Kohistan and Karkoram blocks even after the Shyok suturing process was completed.

According to Le Fort. (1983), Searle et al. (1992) and Fraser et al. (2001) the pre- and syn-collisional subduction of the Neo-Tethys lithosphere and related continental material has produced the majority of the I–type pre-Eocene/Eocene granitoids in the Karakoram terrane. Four stages of magmatic activity have been suggested and reported by previous workers in the Karakoram terrane which are responsible for emplacements of different granitoids. These four stages include calc–alkaline granodiorites during the late Jurassic (~150 Ma; Baig et al. 2021), Tirch Mir granite across the Hindukush (121 – 115 Ma; Heuberger et al. 2007), some parts of the Karakoram Batholith during mid–Cretaceous (105 ± 5 Ma; Fraser et al. 2001) and post-collisional leucogranites (9.6 Ma; (Mahar et al. 2014; Awais et al. 2022, Hussain et al. 2024). The monazite ages from our sample (34 ± 2.2 Ma; granite from HPU, Karakoram Batholith) is in agreement with post–syn collisional granitic intrusion of Mahar et al. (2014), Awais et al. (2022) and Hussain et al. (2024).

BPU in Baltoro region is the part of Karakoram Batholith lies in the east of Karakoram Batholith also yielded young Miocene age (21–26 Ma; Parrish and Tirrul 1989; Scha¨rer et al.

1990; Searle et al. 1992). According to Searle et al. (2010), the Hunza and Baltoro are lying along strike and no suture zone exists between these two regions. This is the reason that both regions preserved magmatic and metamorphic events that are diachronous both in space and time. Using the age concept of Parrish and Tirrul. (1989), Scha¨rer et al. (1990) and Searle et al. (1992) and structural concept of Searl et al. (2010), the studied granite from the HPU are similar to the granites of BPU.

Petrogenesis and Geodynamic Setting of Karakoram Batholith

Tectonic activity in the north Pakistan is very interesting for geologists where the existence of Tethyan Ocean sandwiched between the Indian and Eurasian /Asian plates in the south and north respectively plays a vital role in the subduction related magmatism. Kohistan Batholith and Karakoram Batholith are the two major products of Neo-Tethys Ocean subduction in the south and Paleo–Tethys subduction in the north (Crawford and Searle 1992). There still exists ambuigities for the exact moment and the subduction related magmatism in the KIA and Karakoram Plate. Cao et al. (2016) and Saktura et al. (2021) suggested the initiation of magmatism in the Karakoram approximately 165 to 145 Ma. According to Fraser et al. 2001, the geological development of Tibet lower crust may be significantly highlighted by the detail geology and geochronology of the southern margin of the Eurasian Plate/Asian plate. As the Asian Plate southern margin rocks and Tibet were continues terrane so they assume that magmatic history of the two regions may have been comparable before and after the Indian plate collision (i.e., during and after the early Eocene). Prior to the Indian Plate collision, both areas were magmatically thickened Andean–type plate boundaries with high-temperature andalusite and sillimanite grade metamorphism and huge volumes of granitic-granodioritic magmatism. After continental collision as a result of ongoing north-south compression deep crustal leucogranitic and migmatitic rocks were exhumed from depths of up to 35–45 km in the Karakoram metamorphic complex (Searle and Tirrul, 1991).

The studied rocks of the HPU in the current study share similar chemical characteristics with magmatic rocks of the KIA (south of study area) and Khunjerab Pluton (north of study area) (Ullah et al. 2025). The fractionation of granitoids in HPU seems at shallow depth like Khunjerab pluton in contrast to KIA granitoids where fractionation occurred at deeper depth. Such type of tectonic activity occurs at or very close to the plate boundaries where a relatively older, dense section of ocean floor is pushed beneath a continent resulted in the form of HPU (Fig. 10). This post-India-Asia collisional crustal melt granitic intrusion at the southern margin

of the Karakoram batholith is indicative of Late Eocene-Early Oligocene magmatic activity in the form of HPU (ca. 34 Ma).

Conclusions

The post collisional granitoids of HPU in the Karakoram block are well studied in the context of Petrography, whole rock geochemistry, mineral chemistry and geochronology.

1. Monazite U–Pb data indicates that the HPU granitoids was emplaced at ca. 34 Ma which represents the post/syn–collisional magmtism in the Karakoram Block.
2. The negative relationship between SiO_2 and P_2O_5 and tectonic discrimination plots after Whalen et al. 1987 classified the studied granitoids (HPU, Karakoram Batholith) as I–type granite like KIA granitoids (Kohistan Batholith) and Khunjerab pluton. These I–type HPU granitoids were formed by the partial melting of pre–existing igneous sources, and it is possible that they mixed with mid–crustal rocks of the Karakoram metamorphic complex and/or the ancient Karakoram basement. This is documented by previous interpretations highlighting partial melting of mafic Karakoram lower crust at 26–21 Ma (Mahéo et al. 2009).
3. In comparison and mineralogy of HPU granitoids with KIA granitiods and Khunjerab plutons, the HPU granitoids (Karakoram Batholith) being emplaced at shallow depth like Khunjerab pluton.

Acknowledgment This research is part of the PhD work of the first author. The authors acknowledged the Slovak Academic Information Agency (SAIA) Slovakia for financial support. Monazite dating and Mineral chemistry were performed at Dionýz Štúr State Geological Institute in Bratislava. Ioan Sanilav and Sohaib Ahmad (late) from James Cook University Townsville, Australia are highly acknowledged for performing Scanning Electron Microscopy-Energy Dispersive X-ray Spectroscopy (SEM–EDS) for major elements, Laser ablation–inductively coupled plasma – mass spectrometry (LA–ICP–MS) for the trace and REEs.

Author contributions R.A. and A.A. wrote the main manuscript text. O.N. performed monazite dating and mineral chemistry. M.O. and N.M.M. checked the results, interpretation and reviewed the manuscript thoroughly. M.P. coordinated the research team. M.U. participated in editing the text.

Declaration All authors declare that they have no conflicts of interest related to this study.

References

Abdel–Rahman AM (1994) Nature of biotites from alkaline, calc–alkaline, and peraluminous magmas. J Petrol 35(2):525–541.

Ali M, Zhao KD, Wang C, Rehman HU, Hussain A, Mahar MA, Lutfi W (2024) Geochemical and isotopic constraints on the origin and evolution of the Matum-Das tonalite and mafic enclaves from the Kohistan Batholith, Northern Pakistan. Lithos 470-471(1):107535.

Appleby SK (2008) The origin and evolution of granites: an in–situ study of zircons from Scottish Caledonian intrusions. PhD thesis submitted to The University of Edinburgh.

Appleby SK, Gillespie MR, Graham CM, Hinton RW, Oliver GJ, Kelly NM, EIMF (2010) Do S–type granites commonly sample infracrustal sources? New results from an integrated O, U–Pb and Hf isotope study of zircon. Contrib. Mineral. Petrol. 160:115–132.

Awais M, Liu XC, Qasim M, Wu FY (2022) U(-Th)-Pb age and petrogenesis of Shigar leucogranites, Karakoram Metamorphic Complex, North Pakistan. Geol. J. 57:1–22.

Baig S.S, Xue C, Jan MQ, Rehman, H (2021) Late Jurassic adakite- like granodiorite along the southern Karakoram block, NE Pakistan: new evidence for subduction initiation of the Neo-Tethys Ocean. Lithos 406–407:1–17.

Bowie SHU, Horne JET (1953) Cheralite, a new mineral of the monazite group. Mineral. Mag. 30:93–99.

Boynton WV (1984) Geochemistry of the rare earth elements: Meteorite studies, in Rare Earth Element Geochemistry, edited by P. Henderson, pp. 63–114, Elsevier, New York.

Cao M, Qin K, Li G, Li J, Zhao J, Evans NJ, Hollings, P (2016) Tectono–magmatic evolution of Late Jurassic to Early Cretaceous granitoids in the west central Lhasa subterrane, Tibet. Gondwana Res. 39:386–400.

Chappell BW (1999) Aluminium saturation in I-and S-type granites and the characterization of fractionated haplogranites. Lithos 46(3):535–551.

Chappell BW, White, AJR (2001) Two contrasting granite types: 25 years later. Australian J. Earth Sci. 48(4):489–499.

Chilson-Parks BH, Calabozo FM, Saal AE, Wang Z, Mallick S, Petrinovic IA, Frey, FA (2022) The signature of metasomatized subcontinental lithospheric mantle in the basaltic magmatism of the Payenia volcanic province, Argentina. Geochem. geophys. geosyst. 23(1):10071.

Clemens JD, Wall VJ (1984) Origin and evolution of a peraluminous silicic ignimbrite suite: the Violet Town Volcanics. Contrib. Mineral. Petrol. 88(4):354–371.

Cox KG, Bell JD, Pankhurst RJ (1979) The Interpretation of Igneous Rocks. Allen and Unwin, London, p. 450.

Crawford MB (1988) Leucogranites of the NW Himalaya: Crust–mantle interaction beneath the Karakoram and the magmatic evolution of collisional belts, Ph.D. thesis, University of Leicester, Leicester, England.

Crawford MB, Searle MP (1992) Field relationships and geochemistry of pre–collisional (India–Asia) granitoid magmatism in the central Karakoram, northern Pakistan. Tectonophysics 206:171–192.

Crawford MB, Searle MP (1993) Collision–related granitoid magmatism and crustal structure of the Hunza Karakoram, north Pakistan. In: Treloar, P.J. & Searle, M.P. (eds) Himalayan Tectonics. *Geological Society, London, Special Publications,* 74:53–68.

dos Santos Dias JC, Gonçalves L, Gonçalves CC (2019) Contrasting oxygen fugacity of I-and S-type granites from the Araçuaí orogen, SE Brazil: an approach based on opaque mineral assemblages. Miner. Petrol. 113:667–686.

Debon F, Khan N (1996) Alkaline orogenic plutonism in the Karakorum batholith: the Upper Cretaceous Koz Sar complex (Karambar valley, N. Pakistan). Geodin. Acta. 9(4):145–160.

Debon F, Le Fort P, Dautel D, Sonet J, Zimmermann JL (1987) Granites of western Karakorum and northern Kohistan (Pakistan): a composite Mid–Cretaceous to upper Cenozoic magmatism. Lithos. 20(1):19–40.

Deer WA, Howie RA, Zussman J (1992) An Introduction to the Rock–forming Minerals, 2nd ed. Longman, Hong Kong, p. 712.

Deniel C, Vidal P, Fernandez A, Le Fort P, Peucat JJ (1987) Isotopic study of the Manaslu granite (Himalaya, Nepal): inferences on the age and source of Himalayan leucogranites. Contrib. Mineral. Petrol. 96:78–92.

Förster H–J (1998) The chemical composition of REE–Y–Th–U–rich accessory minerals in peraluminous granites of the Erzgebirge–Fichtelgebirge region, Germany. Part I: the monazite–(Ce)–brabantite solid solution series. Am Mineral 83:259–272. https:// doi.org/10.2138/am–1998–3–409.

Foster MD (1960) Interpretation of the composition of trioctahedral micas. US Geol. Surv. Prof. Pap. 354–B, 1–146.

Fraser JE, Searle MP, Parrish RR, Noble SR (2001) Chronology of deformation, metamorphism, and magmatism in the southern Karakoram Mountains. Geol. Soc. Am. Bull. 113:1443–1455.

Frost BR, Barnes CG, Collins WJ, Arculus RJ, Ellis DJ, Frost CD (2001) A geochemical classification for granitic rocks. J. Petrol. 42 (11):2033–2048.

Gaetani M (1997) The Karakorum block in central Asia, from Ordovician to Cretaceous. Sediment. Geol. *109*(3–4):339–359.

Gagnevin D, Daly JS, Horstwood MSA, Whitehouse MJ (2011) In–situ zircon U–Pb, oxygen and hafnium isotopic evidence for magma mixing and mantle metasomatism in the Tuscan Magmatic Province, Italy. Earth Palnet. Sci. Lett. 305(1–2):45–56.

Gao P, Zheng YF, Zhao ZF (2016) Distinction between S-type and peraluminous I-type granites: Zircon versus whole-rock geochemistry. Lithos 258:77–91.

Goodge JW, Vervoort JD (2006) Origin of Mesoproterozoic A–type granites in Laurentia: Hf isotope evidence. Earth Palnet. Sci. Lett. 243(3–4):711–731.

Green OR, Searle MP, Corfield RI, Corfield RM (2008) Cretaceous–Tertiary carbonate platform evolution and the age of the India–Asia collision along the Ladakh Himalaya (Northwest India). J. Geol. 116:331– 353.

Grove TL, Donnelly-Nolan JM, Housh T (1997) Magmatic processes that generated the rhyolite of Glass Mountain, Medicine Lake volcano, Northern California. Contrib. Mineral. Petrol. 127:205–223.

Grove TL, Elkins-Tanton LT, Parman SW, Chatterjee N, Müntener O, Gaetani, GA (2003) Fractional crystallization and mantle-melting controls on calcalkaline differentiation trends. Contrib. Mineral. Petrol. 145:515–533.

Hacker B, Lufffi P, Lutkov V, Minaev V, Ratschbacher L, Plank T, Metcalf J (2005) Near-ultrahigh pressure processing of continental crust: Miocene crustal xenoliths from the Pamir. J. Petrol. 46(8):1661–1687.

Harris NBW, Ayres M, Massey J (1995) Geochemistry of granitic melts produced during the incongruent melting of muscovite: implications for the extraction of Himalayan leucogranite magmas. J. Geophys. Res. 100:15767–15777.

Harris NBW, Pearce JA, Tindle AG (1986) Geochemical characteristics of collisionzone magmatism. In: Coward, M.P, Rles, A.C. (Eds.), Collision Tectonics. Geol. Soc. Spec. Publ. 19:67–81.

Hawkesworth CJ, Kemp AIS (2006) Using hafnium and oxygen isotopes in zircons to unravel the record of crustal evolution. Chem. Geol. 226(3–4):144–162.

Henry DJ, Guidotti CV, Thomson JA (2005) The Ti-saturation surface for low-tomedium pressure metapelitic biotites: Implications for geothermometry and Tisubstitution mechanisms. Am. Mineral. 90 (2–3):316–328.

Heuberger S, Schaltegger U, Burg JP, Villa IM, Frank M, Dawood H, Zanchi A (2007) Age and isotopic constraints on magmatism along the KarakoramKohistan Suture Zone, NW Pakistan: Evidence for subduction and continued convergence after India-Asia collision. Swiss J. Geosci. 100:85–107.

Hildebrand PR, Noble SR, Searle MP, Parrish RR, Shakiruallah (1998) Tectonic significance of 24 Ma crustal melting in the eastern Hindu Kush, Pakistan. Geology 26:871–874.

Hildebrand PR, Noble SR, Searle, MP, Waters DJ, Parrish RR (2001) Old origin for an active mountain range: Geology and geochronology of the eastern Hindu Kush, Pakistan. Geol. Soc. Am. Bull. 113:625–639.

Hildebrand PR, Searle MP, Shakiruallah Khan Z, Van Hest HJ (2000) Geological evolution of the Hindu Kush, NW Frontier, Pakistan: active margin to continent–continent collision. In: Khan, M.A, Treloar, P.J, Searle, M.P. & Jan, M.Q. (eds) Tectonics of the Nanga Parbat Syntaxis and the Western Himalaya. Geol. Soc. Spec. Publ. 170:277–293.

Hodges KV (2000) Tectonics of the Himalaya and southern Tibet from two perspectives. Geol. Soc. Am. Bull.112:324–350.

Hussain A, Zhao KD, Rehman HU, Sadiq I, Li Q, Baig SS, Hussain SA, Ullah I (2024) Geochronology and petrogenesis of the Miocene S-type Sumayar granite in the Karakoram Block, north Pakistan: Implications for post-collisional magmatism. J. Asian Earth Sci. 264:106053.

Kemp AIS, Foster GL, Schersten Whitehouse MJ, Darling J, Storey C (2009a) Concurrent Pb–Hf isotope analysis of zircon by laser ablation multi–collector ICP–MS, with implications for the crustal evolution of Greenland and the Himalayas. Chem. Geol. 261:244–260.

Kemp AIS, Hawkesworth CJ, Foster GL, Paterson BA, Woodhead JD, Hergt J, Gray CM, Whitehouse MJ (2007) Magmatic and crustal differentiation history of granitic rocks from Hf–O isotopes in zircon. Science 315(5814):980–983.

Kemp AIS, Hawkesworth CJ, Paterson BA, Foster GL, Kinny PD, Whitehouse MJ, Maas T, EIMF (2008) Exploring the plutonic–volcanic link: a zircon U–Pb, Lu–Hf and O isotope study of paired volcanic and granitic units from southeastern Australia. Earth Environ. Sci. Trans. R. Soc. Edinb. 97:337–355.

Kemp AIS, Wormald RJ, Whitehouse MJ, Price RC (2005) Hf isotopes in zircon reveal contrasting sources and crystallization histories for alkaline to peralkaline granites of Temora, southeastern Australia. Geology 33(10):797–800.

Khan SD, Walker DJ, Hall SA, Burke KC, Shah MT, Stockli L (2009) Did the Kohistan-Ladakh island arc collide first with India? Geol. Soc. Am. Bull. 121(3– 4):366–384.

Konečný P, Kusiak MA, Dunkley DJ (2018) Improving U–Th–Pb electron microprobe dating using monazite age references. Chem. Geol. 484:22–35.

Kooijman E, Smit MA, Ratschbacher L, Kylander-Clark ARC (2017) A view into crustal evolution at mantle depths. Earth Planet. Sci. Lett. 465:59–69. https://doi.org/10.1016/j.epsl.2017.02.032.

Kudo AM, Weill DF (1970) An igneous plagioclase thermometer. Contrib. Mineral. Petrol. 25 (1):52–65.

Larson KP, Ali A, Shrestha S, Soret M, Cottle JM, Ahmad R (2019) Timing of metamorphism and deformation in the Swat valley, northern Pakistan: Insight into garnet-monazite HREE partitioning. Geosci. Front. 10:849–861.

Law RD, Searle MP, Godin L (Eds.) (2006) Channel flow, ductile extrusion and exhumation in continental collision zones. Geological Society of London.

Le Fort P (1983) The lower Paleozoic "Lesser Himalayan" granitic belt: emphasis on the Simchar pluton of Central Nepal. Granites of Himalayas, Karakorum and Hindu Kush, 235–255.

Le Fort P, Michard A, Sonet J, Zimmermann JL (1983) Petrography, geochemistry and geochronology of some samples from the Karakoram axial batholith (Northern Pakistan). In: Shams, F.A. (ed.) Granites of the Himalaya, Karakoram and Hindu Kush. Lahore University, Pakistan, 377–387.

Liu PH, Liu FL, Liu CH, Liu JH, Wang F, Xiao LL, Cai J, Shi JR (2014) Multiplr mafic magmatic and high-grade metamorphic events revealed by zircons from meta-mafic rocks in the Daqingshan-Wulashan Complex of the Khondalite Belt, North China Craton. Precambrian Res. 246:334–357.

Lyu P, Liu F, Chen L, Song Z, Ma W, Hou Y (2024) Petrogenesis and tectonic implications of Early Paleozoic granitoids in the Baoshan deposit, Guangxi, South China. Front. Earth Sci. 12:1444751.

Mahar MA, Mah´eo G, Goodell PC, Pavlis TL (2014) Age and origin of post collision Baltoro granites, south Karakoram, North Pakistan: Insights from in-situ U-Pb, Hf and oxygen isotopic record of zircons. Lithos 205:341–358.

Mahéo G, Bertrand H, Guillot S, Villa IM, Keller F, Capiez P (2004) The South Ladakh ophiolites (NW Himalaya, India): an intra–oceanic tholeiitic arc origin with implication for the closure of the Neo–Tethys. Chem. Geol. 203(3–4):273–303.

Mahéo G, Blichert–Toft J, Pin C, Guillot S, Pêcher A (2009) Partial melting of mantle and crustal sources beneath South Karakorum, Pakistan: implications for the Miocene geodynamic evolution of the India–Asia convergence zone. J. Petrol. 50(3):427–449.

Miles AJ, Graham CM, Hawkesworth CJ, Gillespie MR, Hinton RW, Bromiley GD (2014) Apatite: A new redox proxy for silicic magmas?. Geochim. Cosmochim. Acta. 132:101–119.

Molnar P, Lyon–Caen H (1989) Fault plane solutions of earthquakes and active tectonics of the Tibetan Plateau and its margins, *Geophysical Journal International,* 99:123–153.

Nachit H, Ibhi, A, Abia E.H, and Ohoud, M.B, 2005. Discrimination between primary magmatic biotites, re–equilibrated biotites and neoformed biotites. C. R. Geosci. 337:1415–1420.

Ogasawara M, Khan T, Khan F, Kito N, Morishita Y (2004) Ion microprobe U–Pb ages of the Khunjerab granodiorite and some granitoids from Karakoram. Pakistan. Himalayan J. Sci. 2(4):212.

Palin RM, Searle MP, Waters DJ, Horstwood MSA, Parrish RR (2012) Combined thermobarometry and geochronology of peraluminous metapelites from the Karakoram metamorphic complex, North Pakistan: New insight into the tectonothermal evolution of the Baltoro and Hunza Valley regions. J. Metamorph. Geol. 30(8):793–820.

Patiño Douce AE (1999) What Do Experiments Tell Us about the Relative Contributions of Crust and Mantle to the Origin of Granitic Magmas? Geol. Soc. Spec. Publ. London 168:55–75.

Parrish RR, Tirrul R (1989) U–Pb age of the Baltoro granite, northwest Himalaya, and implications for zircon inheritance and monazite U–Pb systematics. Geology 17:1076–1079.

Pearce JA, Harris NB, Tindle AG 1984. Trace element discrimination diagrams for the tectonic interpretation of granitic rocks. J. Petrol. 25:956–983.

Petterson MG, Windley BF (1985) Rb-Sr dating of the Kohistan arc-batholith in the Trans-Himalaya of north Pakistan, and tectonic implications. Earth Planet Sci. Lett. 74(1):45–57.

Petterson MG, Windley BF (1992) The field relationships, geochemistry and petrogenesis of the Cretaceous basalt Jutal dyke suite, Kohistan, N. Pakistan. J. Geol. Soc. London 149:107–114.

Petrík I, Broska I (1994) Petrology of two granite types from the Tríbeč Mountains, Western Carpathians: an example of allanite (+magnetite) versus monazite dichotomy. J. Geol. 29:59–78.

Petrík I, Kohút M (1997) The evolution of granitoid magmatism during the Hercynian orogen in the Western Carpathians. In: Grecula P, Hovorka D. and Putiš M. (Eds.): Geological evolution of the Western Carpathians. Miner. Slovaca—Monograph, Bratislava, 235–252.

Pyle JM, Spear FS, Rudnick RL, McDonough WF (2001) Monazite– Xenotime–garnet equilibrium in metapelites and a new Monazite–Garnet thermometer. J. Petrol 42:2083–2107.

Rex AJ, Searle MP, Tirrul R, Crawford MB, Prior DJ, Rex DC, Barnicoat A (1988) The geochemical and tectonic evolution of the central Karakoram, North Pakistan. Philos. Trans. R. Soc. Lond. A326:229–255.

Ridolfi F (2021) Amp-TB2: An updated model for calcic amphibole thermobarometry. Minerals 11:324.

Robinson AC, Yin A, Manning CE, Harrison TM, Zhang SH, Wang XF (2004) Tectonic evolution of the northeastern Pamir: Constraints from the northern portion of the

Cenozoic Kongur Shan extensional system, western China. Geol. Soc. Am. Bull. 116(7–8):953–973.

Robinson AC, Yin A, Manning CE, Harrison TM, Zhang SH, Wang XF (2007) Cenozoic evolution of the eastern Pamir: Implications for strain–accommodation mechanisms at the western end of the Himalayan–Tibetan orogen. Geol. Soc. Am. Bull. 119(7–8):882–896.

Rolland Y, Pêcher,A, Picard C (2000) Middle Cretaceous back–arc formation and arc evolution along the Asian margin: the Shyok Suture Zone in northern Ladakh (NW Himalaya). Tectonophysics 325:145–173.

Rolland Y, Pêcher A, Picard C, Lapierre H, Bosch D, Keller F, (2002) The Ladakh Arc of NW Himalaya – slab melting and melt–mantle interaction during fast northward drift of Indian Plate. Chem. Geol. 182:139–178.

Saktura WM, Buckman S, Nutman AP, Bennett VC (2021) Late Jurassic Changmar complex from the Shyok ophiolite, NW Himalaya: A prelude to the Ladakh arc. Geol. Mag. 158 (2):239–260.

Scha¨rer U, Copeland P, Harrison TM, Searle MP (1990) Age, cooling history and origin of postcollisional leucogranites in the Karakoram batholith, a multisystem isotope study: J. Geol. 98:233–251.

Schaltegger U, Zeilinger G, Frank M, Burg JP (2002) Multiple mantle sources during island arc magmatism: U–Pb and Hf isotopic evidence from the Kohistan arc complex, Pakistan. Terra Nova 14(6):461–468.

Schärer U, Hamet J, Allègre CJ (1984) The Trans-Himalaya (Gangdese) plutonism in the Ladakh region: a U-Pb and Rb-Sr study. Earth Planet. Sci. Lett. 67(3):327– 339.

Schwab M, Ratschbacher L, Siebel W, McWilliams M, Minaev V, Lutkov V, Chen F, Stanek K, Nelson B, Frisch W, Wooden JL (2004) Assembly of the Pamirs: Age and origin of magmatic belts from the southern Tien Shan to the southern Pamirs and their relation to Tibet. Tectonics 23(4):1–31.

Searle M, Crawford M, Rex A (1992) Field relations, geochemistry, origin and emplacement of the Baltoro granite, central Karakoram. Earth Environ. Sci. Trans. R. Soc. Edinb. 83:519–538.

Searle MP, Tirrul R (1991) Structural and thermal evolution of the Karakoram crust. J. Geol. Soc. Lond. 148:65–82.

Searle MP (1991) Geology and tectonics of the Karakoram Mountains: Chichester, J. Wiley and Sons, 358.

Searle MP (2011) Geological evolution of the Karakoram Ranges. Ital. J. Geosci. 130(2):147–159.

Searle MP, Khan MA (1996) Geological Map of North Pakistan and Adjacent Areas of Northern Ladakh and Western Tibet, 1:650,000. Oxford, England: Oxford University.

Searle MP, Cooper DJW, Rex AJ (1988) Collision tectonics of the Ladakh–Zanskar Himalaya. Philos. Trans. R. Soc. Lond. A326:117–150.

Searle MP, Law RD, Jessup MJ (2006) Crustal structure, restoration and evolution of the Greater Himalaya in Nepal–South Tibet: implications for channel flow and ductile extrusion of the middle crust. Geol. Soc. Lond. Spec. Publ. 268(1):355–378.

Searle MP, Parrish RR, Thow AV, Noble SR, Phillips, RJ, Waters DJ (2010) Anatomy, age and evolution of a collisional mountain belt: the Baltoro granite batholith and Karakoram Metamorphic Complex, Pakistani Karakoram. J. Geol. Soc. 167(1):183–202.

Searle MP, Rex AJ, Tirrul R, Rex DC, Barnicoat A (1989) Metamorphic, magmatic and tectonic evolution of the Central Karakoram in the Biafo–Hushe regions of N. Pakistan. In: Malinconico, L. Jr. & Lillie, R.J. (eds) Tectonics of the western Himalaya. Geol. Soc. Am. 232:47–74.

Searle MP, Simpson RL, Law, RD, Parrish RR, Waters DJ (2003) The structural geometry, metamorphic and magmatic evolution of the Everest massif, High Himalaya of Nepal–South Tibet. J. Geol. Soc. 160(3):345–366.

Searle MP, Waters DJ, Dransfield MW, Stephenson BJ, Walker CB, Walker JD, Rex DC (1999) Thermal and mechanical models for the structural and metamorphic evolution of the Zanskar High Himalaya. In: Mac Niocaill, C, Ryan, P.D. (Eds.), Continental Tectonics. Geol. Soc. Lond. Spec. Publ. 164:139–156.

Shaw SE, Flood RH (2009) Zircon Hf isotopic evidence for mixing of crustal and silicic mantle–derived magmas in a zoned granite pluton, eastern Australia. J. Petrol. 50(1):147–168.

Shellnutt JG (2018) Derivation of intermediate to silicic magma from the basalt analyzed at the Vega 2 Tlanding site, Venus. PloS One 13(3): 194155.

Soret M, Larson KP, Cottle JM, Smit M, Johnson A, Shrestha S, Ali A, Faisal S (2019) Mesozoic to Cenozoic tectono-metamorphic history of the South Pamir–Hindu Kush (Chitral, NW Pakistan): Insights from phase equilibria modelling, and garnet–monazite petrochronology: J. Metamorph. Geol. 118, 1.

Stuckless John S (1989) Petrogenesis of Two Contrasting, Late Archean Granitoids, Wind River Range, Wyoming. No. 1491. US Government Printing Office.

Sun SS, McDonough WF (1989) Chemical and isotopic systematics of oceanic basalts: implications for mantle composition and processes. In A. D. Saunders, and M. J. Norry (Editors). Chemical and isotopic systematics of oceanic basalts: implications for mantle composition and processes, (London, Special Publications). 42(1):313–345. doi:10.1144/gsl.sp.1989.042.01.19

Thompson RN (1982) Magmatism of the British Tertiary volcanic province. Scot. J. Geol. 18(1):49–107.

Tischendorf G, Gottesmann B, Förster HJ, Trumbull RB (1997) On Li–bearing micas: estimating Li from electron microprobe analyses and an improved diagram for graphical representation. Min. Mag. 61:809–834.

Todd VR, Shaw SE (1985) S–type granitoids and an I–S line in the Peninsular Ranges batholith, southern California. Geology 13:231–233.

Ullah M, Klötzli U, Rentenberger C, Sláma J, Younas M, Khubab M, Goudarzi M, Ahmad T (2025) Unravelling the geochemical and geochronological diversities of the pre–

collisional magmatism: Implications for the subduction dynamics in the Kohistan island arc and Karakorum block, Pakistan. Geoci. Front. 16:102003.

Valley JW, Lackey JS, Cavosie AJ, Clechenko CC, Spicuzza MJ, Basei MAS, Wei, CS (2005) 4.4 billion years of crustal maturation: oxygen isotope ratios of magmatic zircon. Contrib. Mineral. Petrol. 150:561–580.

Warr LN (2021) IMA–CNMNC approved mineral symbols. ***Min. Mag.*** 85:291–320. https://doi.org/10.1180/mgm. 2021.43.

Weinberg RF, Dunlap W, Whitehouse M, (2000) Newfield, structural and geochronological data from the Shyok and Nubra valleys, northern Ladakh: linking Kohistan to Tibet. In: Khan, M.A, Treloar, P.J, Searle, M.P, Jan, M.Q. (Eds.), Tectonics of the Nanga Parbat Syntaxis and theWestern Himalaya. Geol. Soc. Lond. Spec. Publ. 170:253–275.

Whalen JB, Currie KL, Chappell BW (1987) A–type granites: geochemical characteristics, discrimination and petrogenesis. Contrib. Mineral. Petrol. 95:407–419.

Wolf MB, London D (1994) Apatite dissolution into peraluminous haplogranitic melts: an experimental study of solubilities and mechanisms. Geochim. Cosmochim. Acta. 58(19):4127–4145.

Wones DR (1989) Significance of the assemblage titanite+ magnetite+ quartz in granitic rocks. Am. Mineral. 74 (7–8):744–749.

Wu H, Xie C, Li C, Wang M, Fan, J Xu W (2016) Tectonic shortening and crustal thickening in subduction zones: Evidence from Middle–Late Jurassic magmatism in Southern Qiangtang, China. Gondwana Res. 39:1–13.

Zeh A, Gerdes A, Klemd R, Barton JM Jr (2007) Archaean to Proterozoic crustal evolution in the Central Zone of the Limpopo Belt (South Africa–Botswana): Constraints from combined U–Pb and Lu–Hf isotope analyses of zircon. J. Petrol. 48:1605–1639.

Zeitler PK (1985) Cooling history of the NW Himalaya, Pakistan. Tectonics 4:127–151.

Zhu B, Kidd WSF, Rowley DB, Currie BS, Shafique N (2005) Age of initiation of the India–Asia collision in the east central Himalaya. J. geol. 113:265–285.

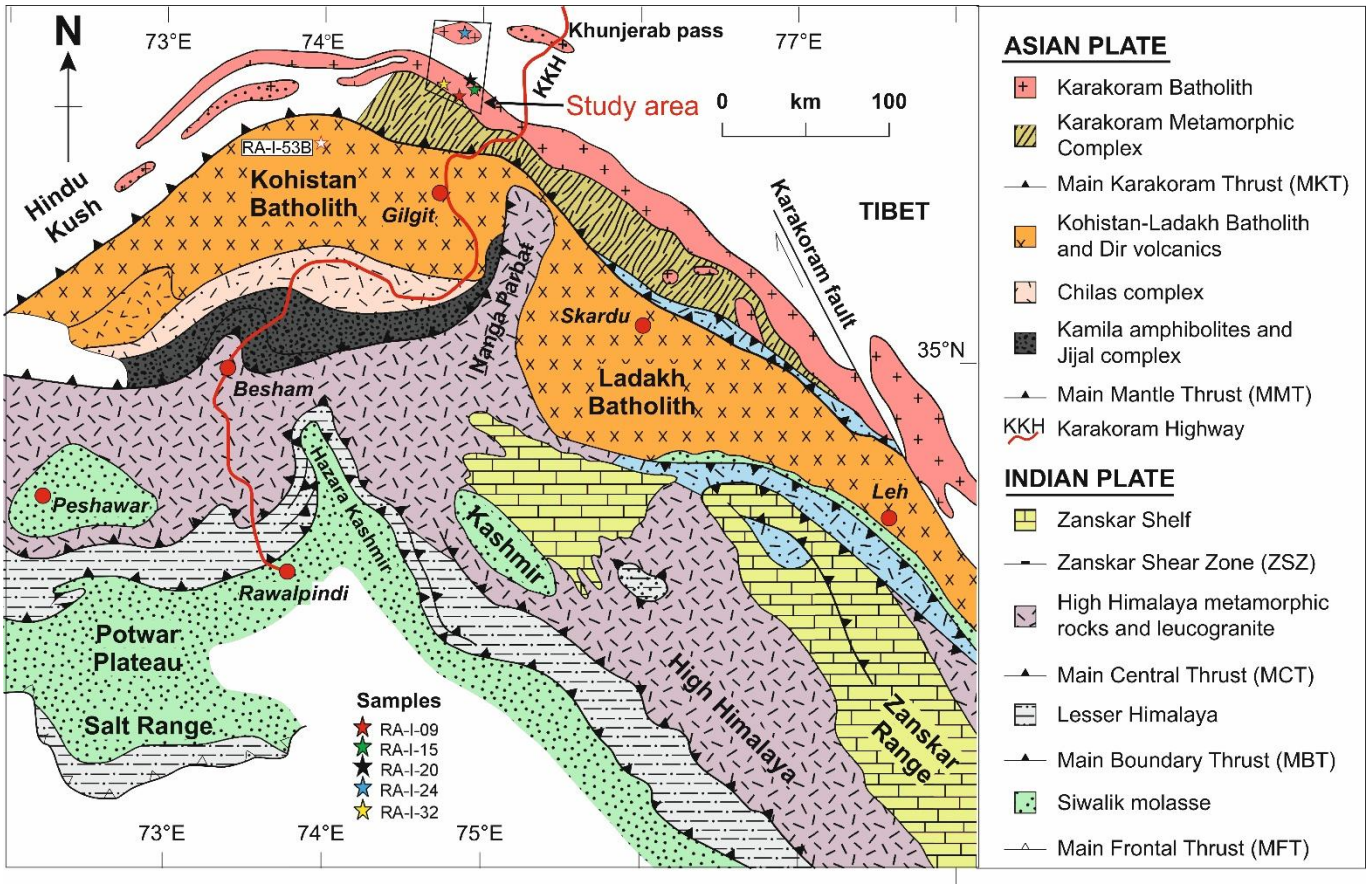


Figure 1. Generalized geological map displaying the position of the Hunza Valley in relation to the rest of the Karakoram (after Searle et al. 1999). The GPS locations of samples are as follow; 36°16'42"N 74°42'55"E (sample RA–I–09), 36°19'02"N 74°52'56"E (sample RA–I–15), 36°23'27"N 74°50'57"E (sample RA–I–20), 36°47'18"N 74°53'25"E (sample RA–I–24), 36°20'26"N 74°34'30"E (RA–I–32) and 36°09'37"N 73°50'21"E (RA–I–53B).

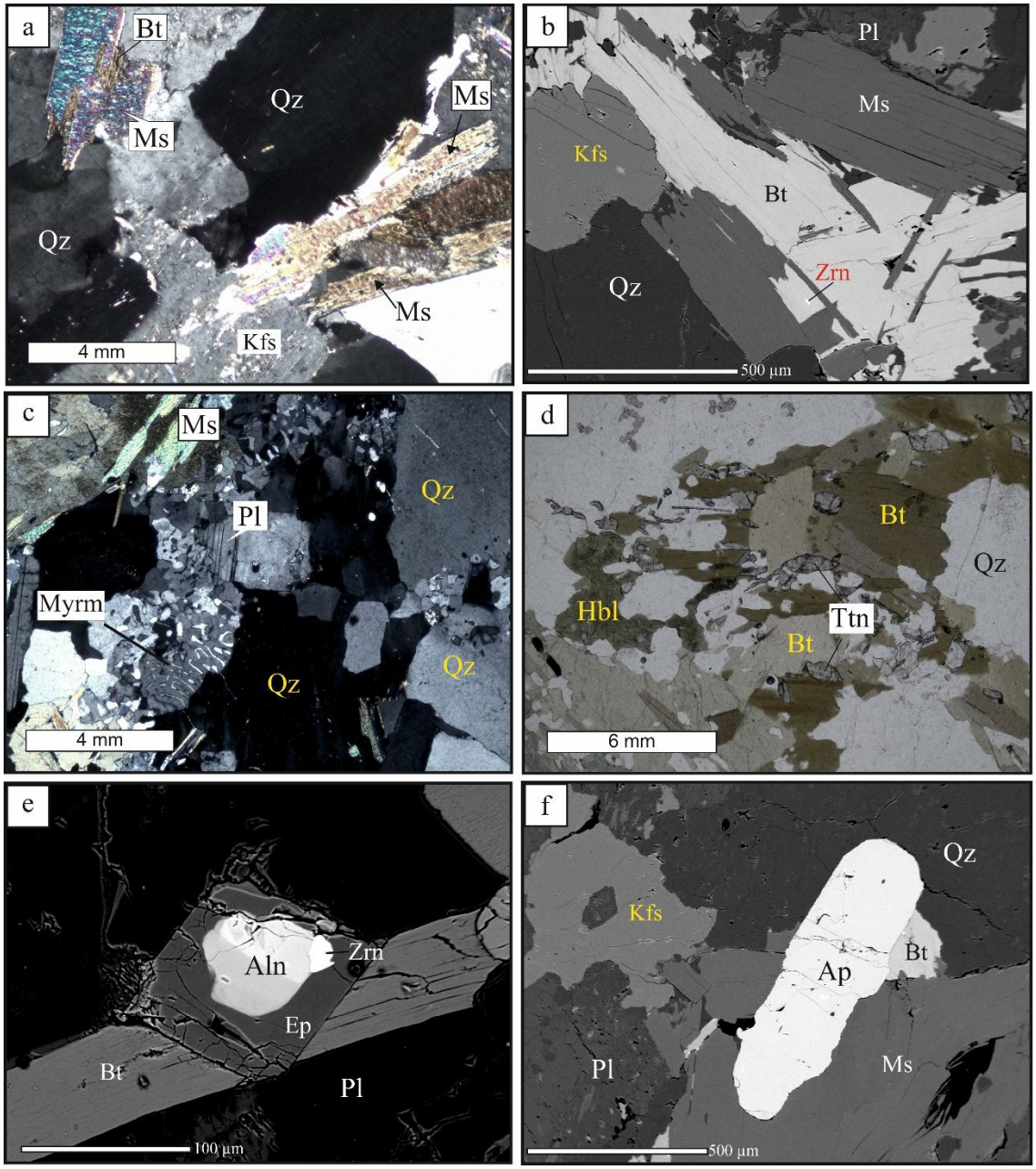


Figure 2. (a) Photomicrpgraph showing euhedral to subhedral quartz (Qz), inclusions of muscovite (Ms) and biotite (Bt). The fractures in K-feldspar (Kfs) are filled with micro crystalline quartz (Qz). (b) Back Scattered Electron (BSE) image of the rock forming and accessory minerals and tectures. (c) Myrmekites (Myrm) with well-developed vermicular intergrowth are common in plagioclase (Pl) (d-f) BSE image showing the distribution of epidote

(Ep), zircon (Zrn), titanite (Ttn), allanite (Aln) and apatite (Ap) in the studied samples. IMA-CNMNC approved mineral symbols according to Warr (2021).

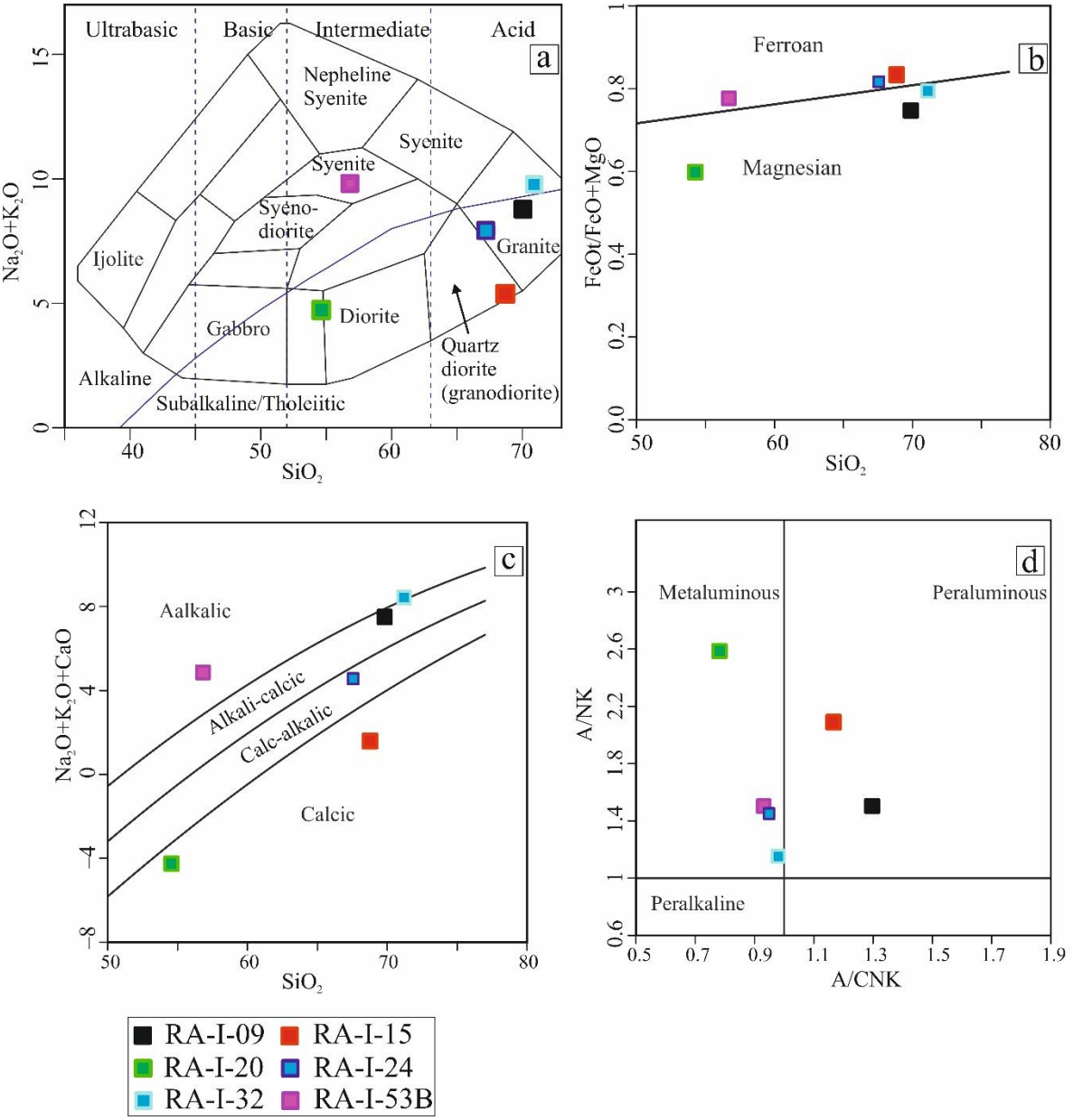


Figure 3. (a) Compositional classification of studied granitoid rocks using major elements characteristics (after Cox et al. 1979). (b, c) Geochemical affinity determination using the Frost et al. 2001 classification and (d) Binary plot of A/NK vs. A/CNK afetr Patiño Douce (1999). A/NK = (Al_2O_3/Na_2O + K_2O) A/CNK = (Al_2O_3/CaO+Na_2O+K_2O).

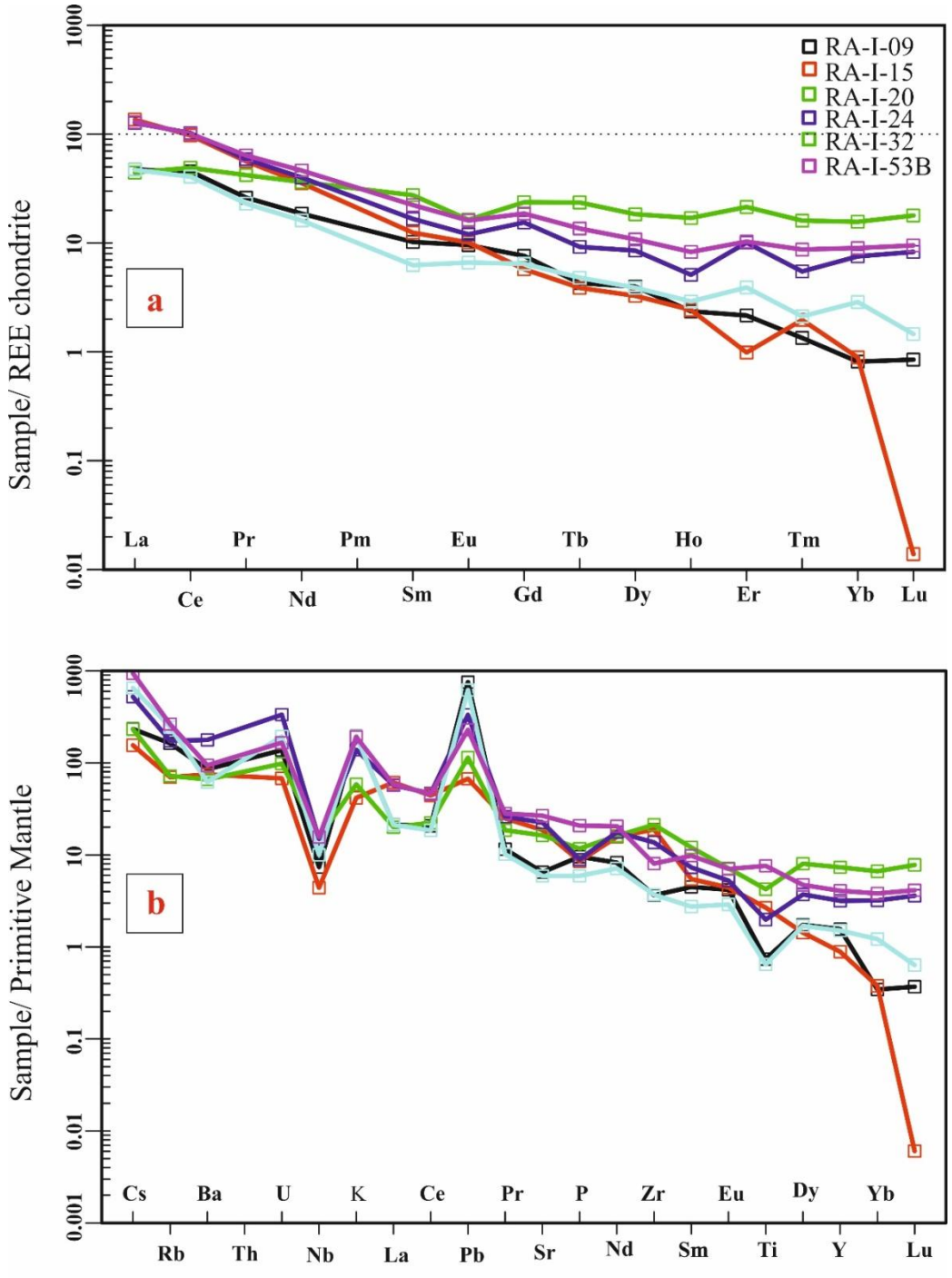


Figure 4. (a) Chondrite-normalized REE pattern (after Boynton 1984) (b) primitive–mantle–normalized trace element patterns (after Sun and McDonough 1989) for granitoid rocks of HPU from Karakoram batholith.

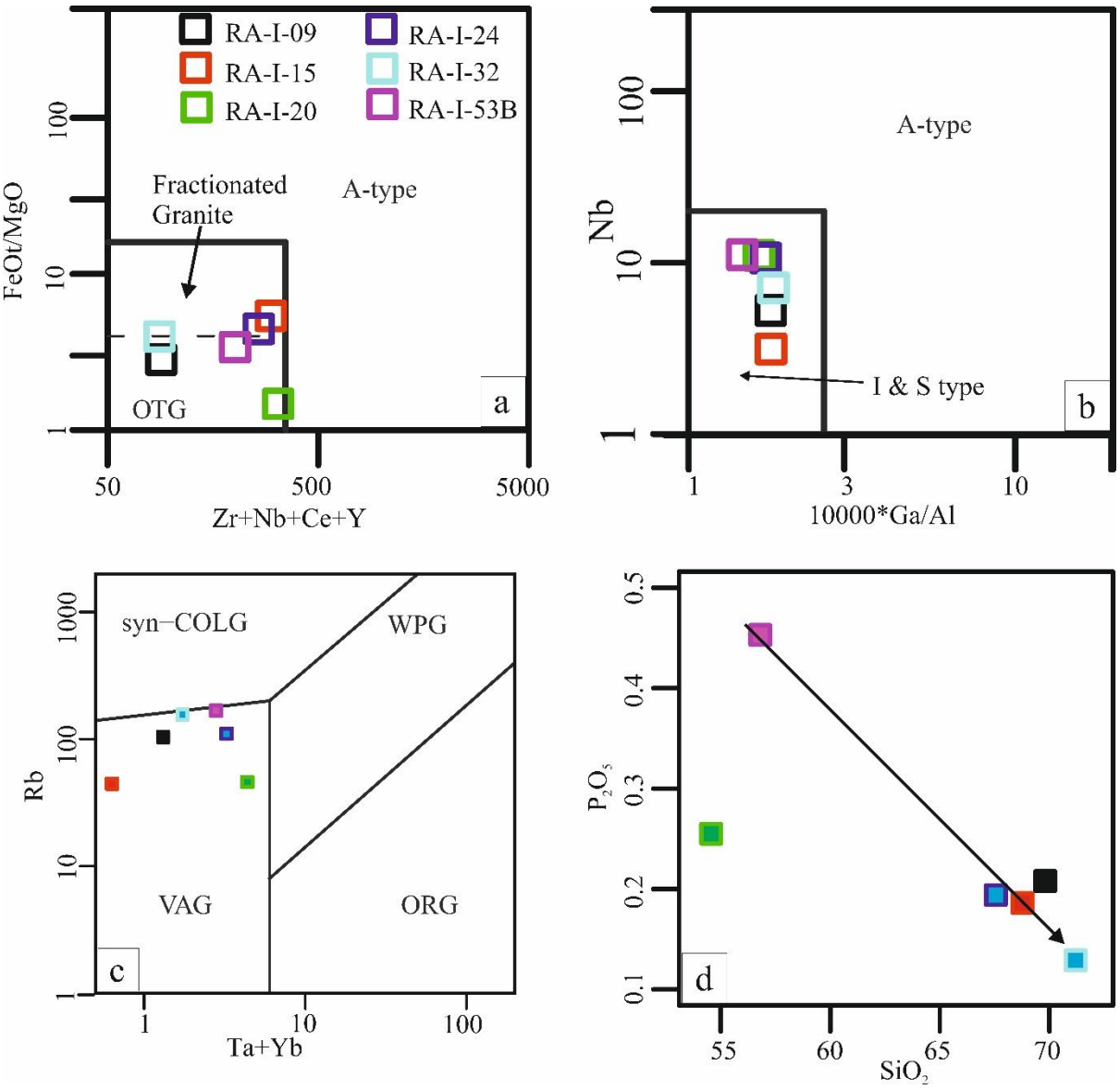


Figure 5. (a) Binary plot of Zr + Nb + Ce + Y vs. FeOt /MgO. (b) Binary plot of Ce vs. 10000∗Ga/Al diagrams for studied rocks (Whalen et al. 1987). (c) Binary plot of Y+Nb vs. Rb (Pearce et al. 1984). Abbreviations: Syn-collisional Granite (syn–COLG), Post-collisional Granite (post–COLG), Volcanic Arc Granite (VAG), Within Plate Granite (WPG), Oceanic Ridge Granite (ORG) (d) Relation between SiO_2 and P_2O_5 (symbols in d are the same as in Figure 3).

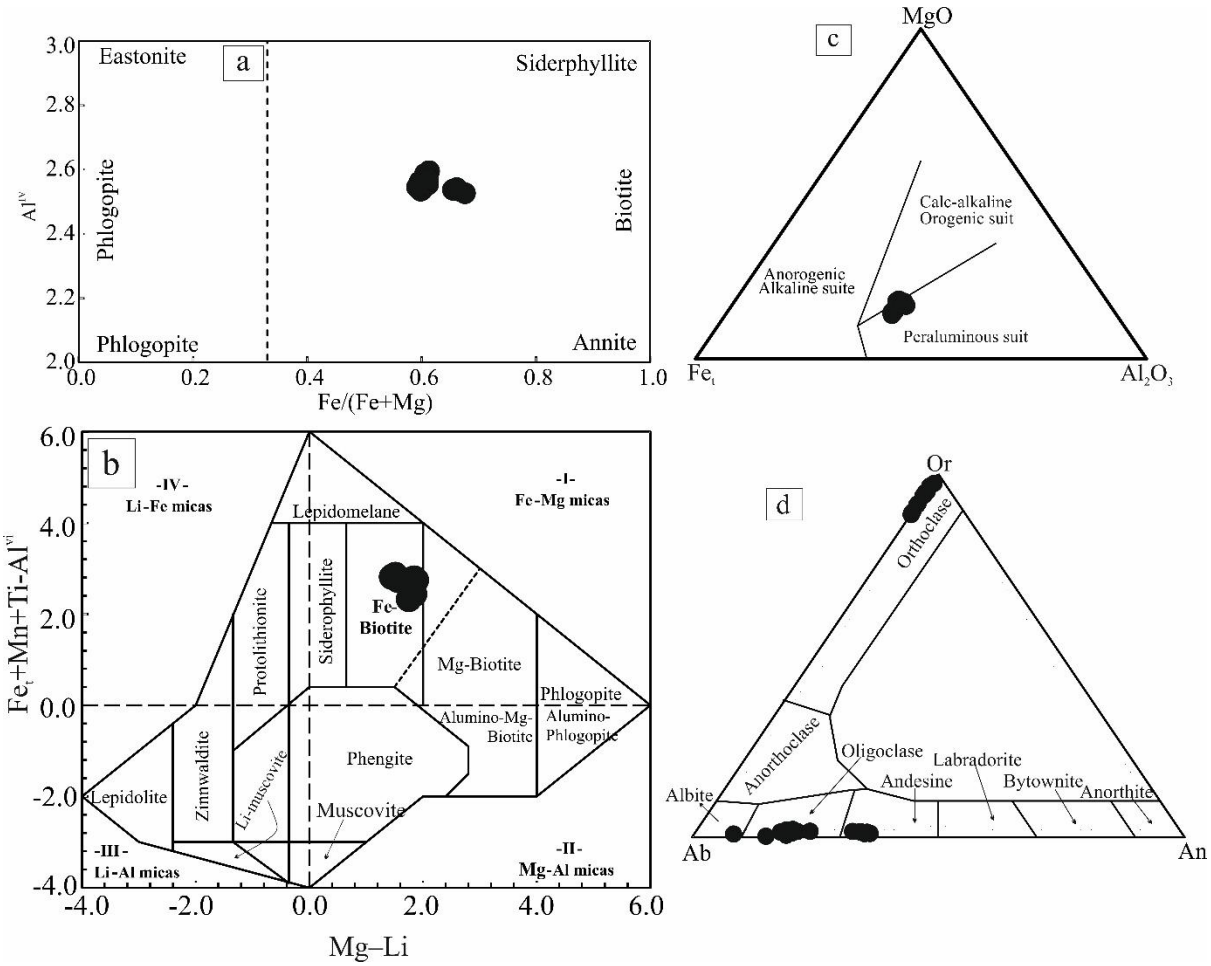


Figure 6. Chemical composition of biotites from the HPU, Karakoram Batholith on classification diagrams. (a) Fe/(Fe + Mg) vs. Al^{IV} (after Deer et al. 1992); (b) after Tischendorf et al. (1997). (c) Compositional classification of biotites from HPU on (a) MgO–FeO_t–Al_2O_3 diagram (after Abdel-Rahman 1994). (d) Classification of feldspars ternary orthoclase-albite-anorthite diagram.

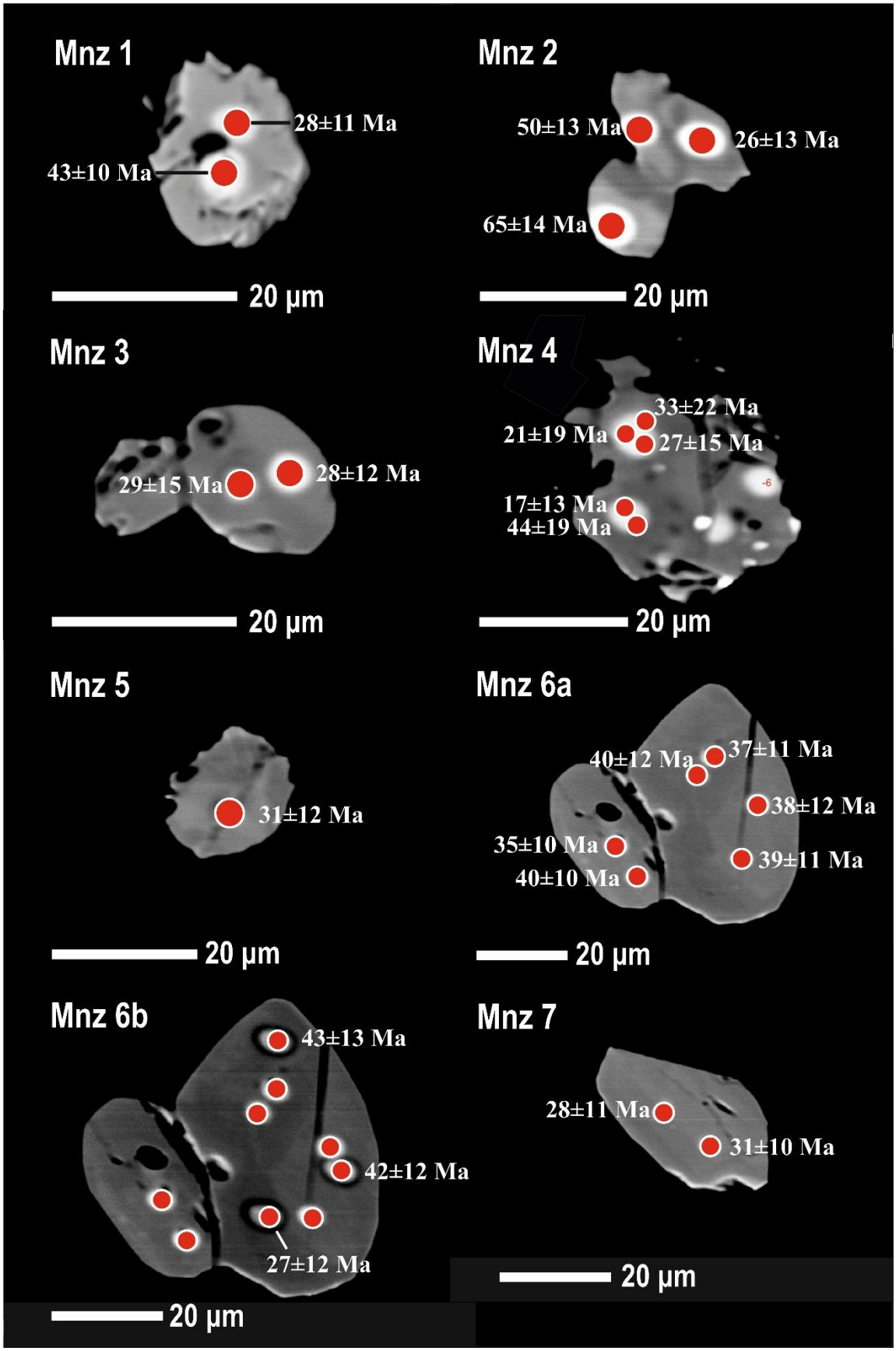
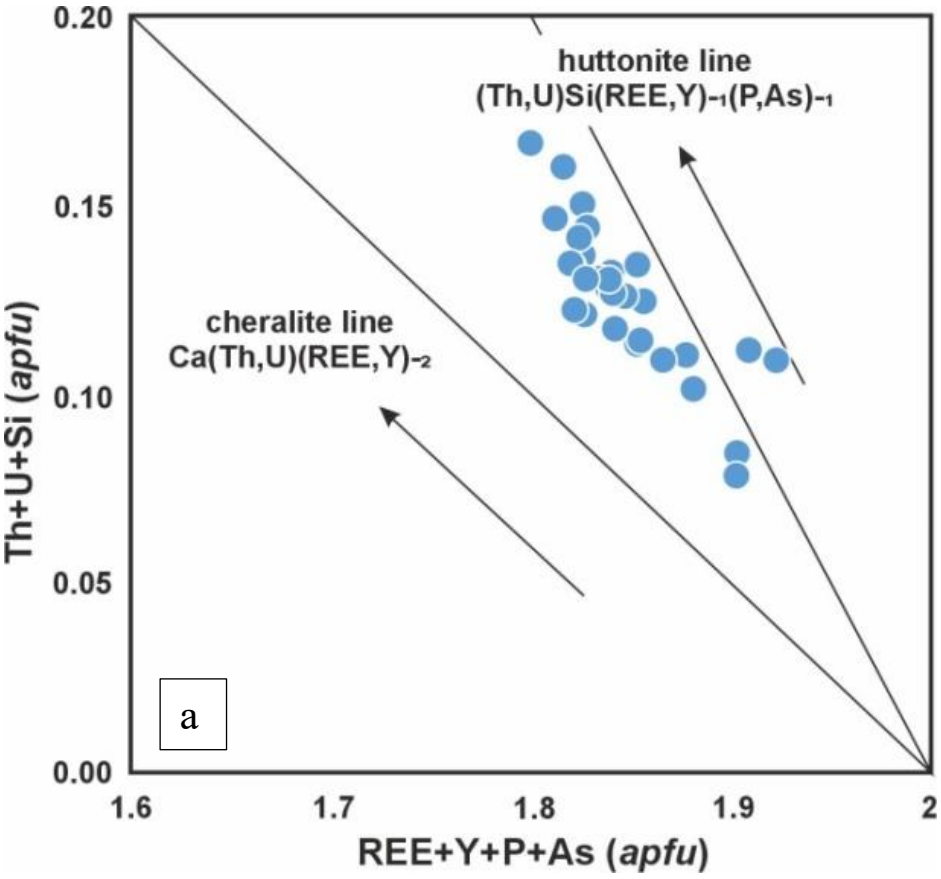
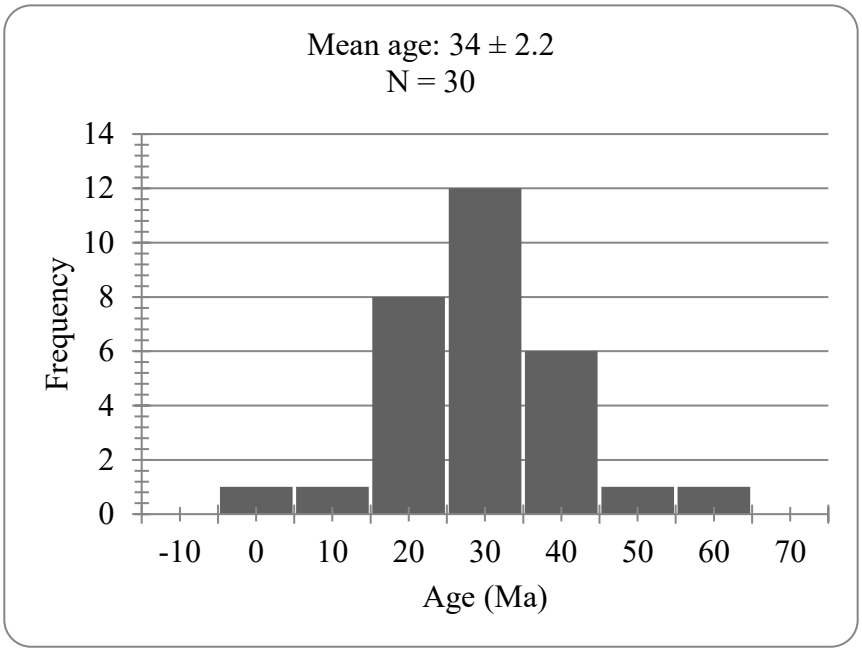

Mnz 1
28±11 Ma
43±10 Ma
20 µm
Mnz 2
50±13 Ma
26±13 Ma
65±14 Ma
20 µm
Mnz 3
29±15 Ma
28±12 Ma
20 µm
Mnz 4
33±22 Ma
21±19 Ma
27±15 Ma
17±13 Ma
44±19 Ma
20 µm
Mnz 5
31±12 Ma
20 µm
Mnz 6a
40±12 Ma
37±11 Ma
38±12 Ma
35±10 Ma
39±11 Ma
40±10 Ma
20 µm
Mnz 6b
43±13 Ma
42±12 Ma
27±12 Ma
20 µm
Mnz 7
28±11 Ma
31±10 Ma
20 µm

Figure 7. BSE of monazite grains from sample RA–I–32 with analytical spots of EPMA in-situ dating.





b

Figure 8. (a) Compositions of monazite -(Ce) in Th + U + Si vs. REE + Y + P + As subsitution diagram (atomic proportions) with ideal substitution vectors (c) Histograms of monazite ages. These plots are from sample RA–I–32, HPU Karakoram Batholith.

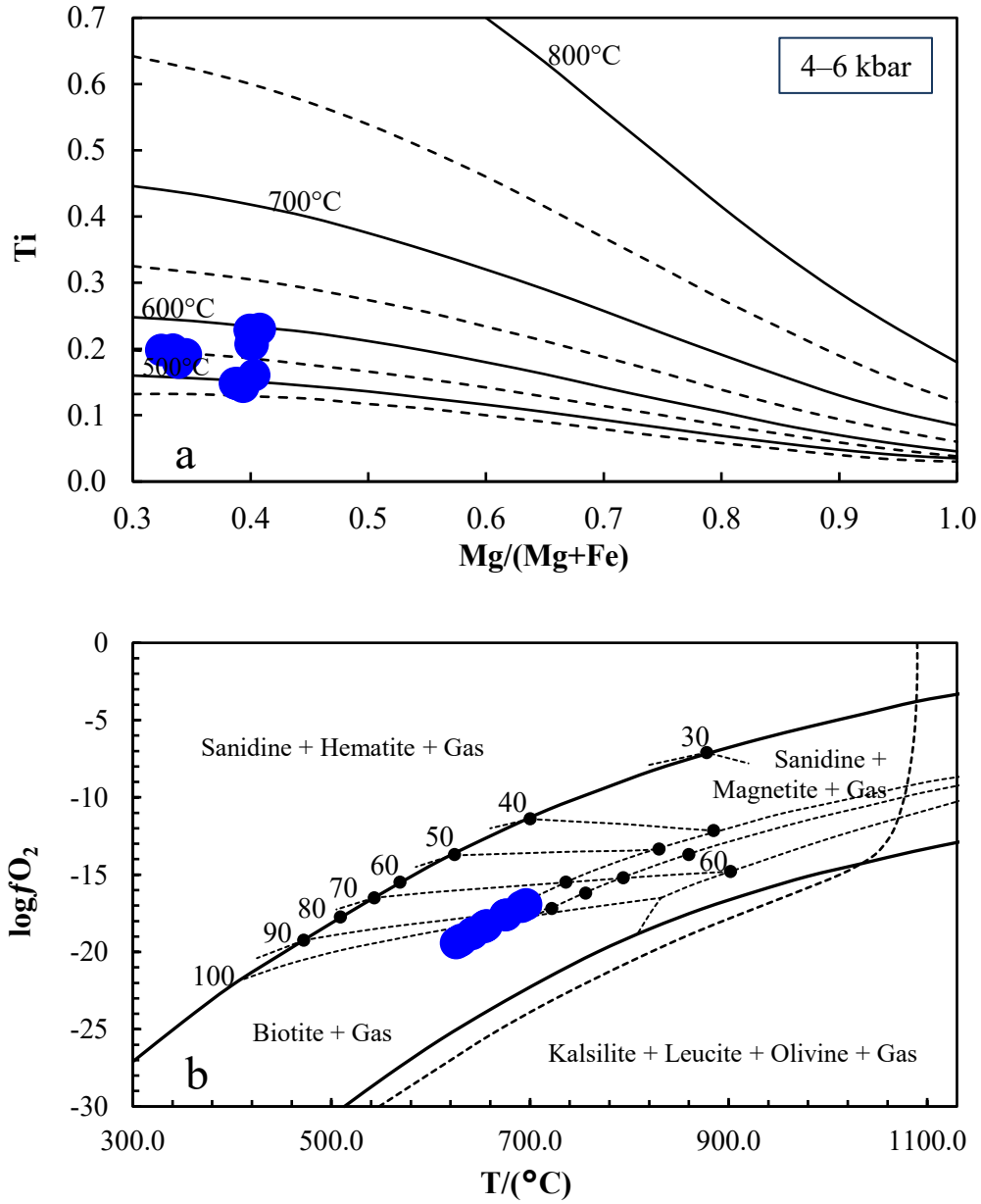


Figure 9. (a) Ti against Mg/(Mg + Fe) ratio in the biotite composition from the HPU Karakoram batholith (after Henry et al. 2005) and (b) show the logfO_2 vs. T (ºC) estimated from the mineralogical composition using the same biotites. The dotted lines demonstrate the probability in percent of the biotite + gas buffer (Wones, 1989).

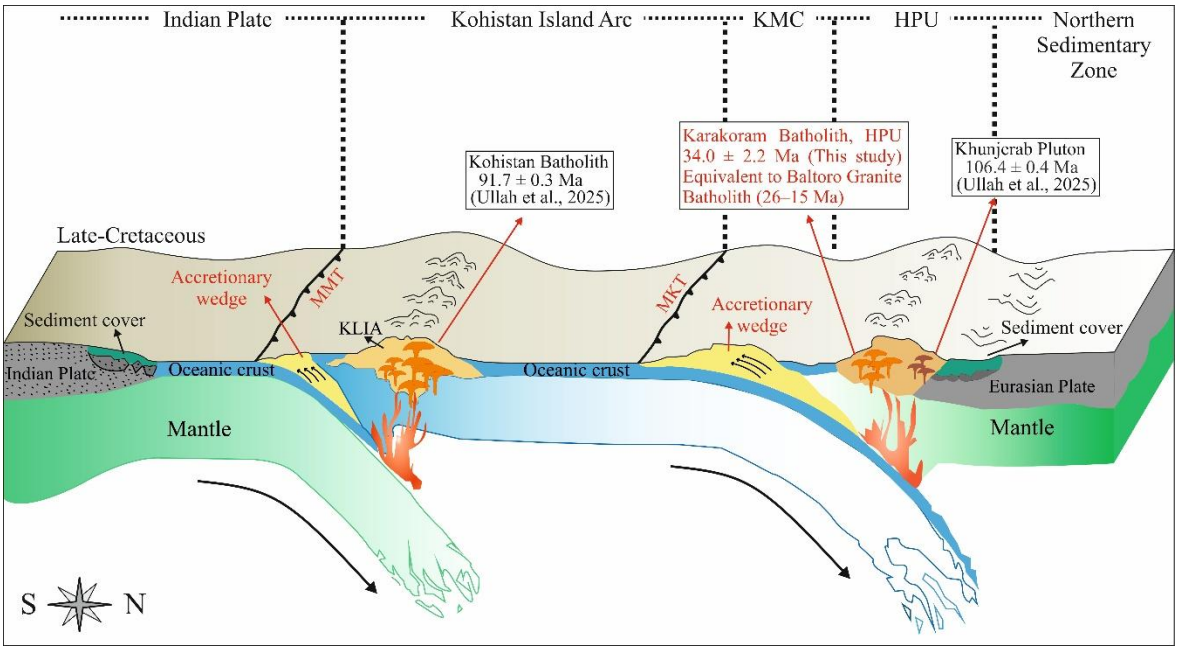


Figure 10. Schematic tectonic model (not to scale) (modified after Ullah et al. 2025) showing the emplacement of HPU (Karakoram Batholith) and surrounding batholiths in north Pakistan.

Supplementary Files

This is a list of supplementary files associated with this preprint. Click to download.

- Tablesonly.docx